Effects of spin-dependent quasiparticle renormalization in Fe, Co, and Ni photoemission spectra: An experimental and theoretical study

J. Sánchez-Barriga,[1] J. Braun,[2] J. Minár,[2] I. Di Marco,[3] A. Varykhalov,[1] O. Rader,[1] V. Boni,[4] V. Bellini,[5] F. Manghi,[4] H. Ebert,[2] M. I. Katsnelson,[6] A. I. Lichtenstein,[7] O. Eriksson,[3] W. Eberhardt,[1] H. A. Dürr,[1,8] and J. Fink[1,9]

[1]*Helmholtz-Zentrum Berlin für Materialien und Energie, Elektronenspeicherring BESSY II, Albert-Einstein-Strasse 15, D-12489 Berlin, Germany*

[2]*Dep. Chemie und Biochemie, Physikalische Chemie, Universität München, Butenandtstr. 5-13, D-81377, München, Germany*

[3]*Department of Physics and Astronomy, Box 516, SE-751 20, Uppsala, Sweden*

[4]*Dipartimento di Fisica, Università di Modena, Via Campi 213/a, I-41100 Modena, Italy*

[5]*S3 – Institute of Nanoscience – CNR, Via Campi 213/A, I-41125 Modena, Italy*

[6]*Institute of Molecules and Materials, Radboud University of Nijmegen, Heijendaalseweg 135, 6525 AJ Nijmegen, The Netherlands*

[7]*Institute of Theoretical Physics, University of Hamburg, D-20355 Hamburg, Germany*

[8]*Pulse Institute and Stanford Institute for Energy and Materials Science, SLAC National Accelerator Laboratory, Menlo Park, California 94025, USA*

[9]*Leibniz-Institute for Solid State and Materials Research Dresden, P.O. Box 270116, D-01171 Dresden, Germany*

(Received 6 March 2012; published 7 May 2012)

We have investigated the spin-dependent quasiparticle lifetimes and the strength of electron correlation effects in the ferromagnetic 3*d* transition metals Fe, Co, and Ni by means of spin- and angle-resolved photoemission spectroscopy. The experimental data are accompanied by state-of-the-art many-body calculations within the dynamical mean-field theory and the three-body scattering approximation, including fully relativistic calculations of the photoemission process within the one-step model. Our quantitative analysis reveals that inclusion of local many-body Coulomb interactions are of ultimate importance for a realistic description of correlation effects in ferromagnetic 3*d* transition metals. However, we found that more sophisticated many-body calculations with larger modifications in the case of Fe and Co are still needed to improve the quantitative agreement between experiment and theory. In general, it turned out that not only the dispersion behavior of energetic structures should be affected by nonlocal correlations but also the line widths of most of the photoemission peaks are underestimated by the current theoretical approaches. The increasing values of the on-site Coulomb interaction parameter U and the band narrowing of majority spin states obtained when moving from Fe to Ni indicate that the effect of nonlocal correlations becomes weaker with increasing atomic number, whereas correlation effects tend to be stronger.

DOI: 10.1103/PhysRevB.85.205109 PACS number(s): 75.70.Rf, 71.15.Mb, 73.20.At, 79.60.Bm

I. INTRODUCTION

Over decades, the underlying mechanisms giving rise to the electronic structure and magnetism of correlated systems have received continuous scientific attention. However, a detailed understanding of the dispersion behavior of electronic states, for example, in transition metal compounds such as cuprate or pnictide high-T_c superconductors,[1,2] 4*f* rare-earth systems,[3] or 3*d* transition metals[4] is still missing. In the case of ferromagnetic transition metals, an extensive experimental work in this respect has been carried out over the last 30 years.[5–13] At present, for a detailed understanding of the manifestation of spin-dependent electronic correlations, Fe, Co, and Ni serve as prototype systems of moderately correlated 3*d* materials because their electronic structure in the vicinity of the Fermi level is dominated by spin-polarized *d* bands.

On the other hand, due to the presence of correlation effects, a quantitative description of the corresponding band structures of Fe, Co, and Ni has been a long-standing theoretical problem which has not been solved completely, particularly in relation to experimentally obtained band dispersions, quasiparticle lifetimes, and Fermi surfaces. Major reasons for this are found in the mass renormalization of electronic states due to correlation effects and, close to the Fermi level, in the coupling of the charge carriers to bosonic excitations such as phonons, magnons, and plasmons. All these phenomena taken together form the basis for a detailed microscopic understanding of the transport properties and the magnetic properties of transition metals. Moreover, material design on the nanometer scale is intimately connected to this knowledge. Experimentally, the energy region around the Fermi edge can be probed in detail by means of (spin-dependent) angle-resolved photoemission spectroscopy [(S)ARPES] and inverse photoemission. Important experimental progress had been achieved in this field and in related spectroscopies.[14] Modern experimental arrangements supply not only spin resolution but also extremely high angle and energy resolutions, and consequently, reveal details of the spin-dependent dispersing spectral function very close to the Fermi level.

On the theoretical side, the application of density functional theory (DFT) in the local density approximation (LDA)[15] has contributed with numerous calculations of single-particle $E(\mathbf{k})$ band dispersions of solids, surfaces, and ultrathin films. However, a comprehensive understanding of the underlying physics of such materials and a quantitative analysis of correlation effects requires a realistic calculation of excitation spectra that are in general not well described by single-particle approaches such as the local spin-density approximation

(LSDA) or the generalized gradient approximation (GGA)[16] in DFT. More recently, theories beyond DFT have been developed to take many-body interaction (i.e., correlation effects) in a more quantitative way into account. In this context we mention the dynamical mean-field theory (DMFT)[17–19] which replaces the problem of describing correlation effects in a periodic lattice by a correlated impurity coupled to a self-consistent bath and an alternative approach, the three-body scattering (3BS) approximation[20] which takes into account the relaxation of a hole by an Auger-like excitation in the valence band, formed by one hole plus an electron-hole excitation using a *T*-matrix formalism. Both theories allow calculating an approximated momentum and energy-dependent spectral function which is described by the bare-particle band structure and the complex self-energy function Σ. The real part of Σ is related to the mass renormalization [i.e., the reduction of the binding energy (BE) relative to the bare-particle dispersion]. The imaginary part of Σ which is related to the inverse finite lifetime of the quasiparticles, determines the broadening of the spectral function along a certain momentum direction at constant energy. Often, the mass renormalization is separated in two contributions: a low-energy contribution caused by a coupling of charge carriers to low-energy bosonic excitations such as phonons and magnons and a high-energy electronic contribution due to correlation effects.

Early attempts to compare experiment and theory indicated that for Co—but also for Fe—many-body effects can be considered to be small.[8,12] In contrast, for Ni, band structure calculations could not describe the photoemission satellite at 6-eV BE and, in addition, compared to the LSDA band structure calculations of the 3*d* bands, a substantial (high-energy) mass-enhancement factor between 1.3 and 1.5 was obtained.[21–26] More recent (S)ARPES studies revealed also for Fe and Co considerable many-body effects. For Fe at high binding energies mass renormalizations up to a factor of 1.3 have been detected.[27,28] It has been shown that very close to the Fermi energy mass renormalizations are even higher, reaching values up to 3.6.[28–30] Moreover a strong broadening of the ARPES peaks in Fe has been observed amounting to about 60% of the BE.[27] Most recently, we have published a detailed comparison of SARPES measurements and DMFT/3BS calculations on Fe indicating that the present state-of-the art many-body calculations still underestimate correlation effects.[31] The discrepancy has been explained in terms of a strong nonlocality of correlation effects not taken into account in the present DMFT/3BS calculations. In the case of Co, which has been at the focus of (S)ARPES experiments since the beginning of the 1980s,[8,32–38] only a few studies have been devoted to a detailed comparison between many-body calculations and experiments.[32,35,39–41] Here we point out that SARPES revealed a strong spin dependence of the scattering rates at high BE (i.e., the bulklike Co majority spin bands show a much larger broadening when compared to the corresponding bulklike minority bands for binding energies larger than $\sim$1 eV).[40] On the other hand, most recent spin- and time-resolved two-photon photoemission experiments in fcc Co films indicated a negligible spin dependence of the scattering rates of hot electrons emitted from the Co surface state located at a BE of $\sim$0.4 eV.[42] This effect was explained in terms of a dominance of exchange scattering processes at around that BE.[42]

Early theoretical attempts to take into account correlation effects in the electronic structure of 3*d* transition metals were reviewed by Davis.[8] Among the various more recent attempts to calculate the influence of correlation effects on the spectral function of the ferromagnetic 3*d* transition metals we mention here recent DMFT calculations[18,31,40,43] on Fe, Co, and Ni, 3BS calculations on Fe and Co[31,39,40] and Gutzwiller theory[44,45] calculations on Ni.[26]

In the present work we focus on SARPES studies on Ni and combine them with extended results of our previous SARPES studies[31,40] on Fe and Co to give a complete comparative overview on how spin-dependent electronic correlations influence the ferromagnetic 3*d* transition metal series. We emphasize that we cannot resolve the low-energy contributions to the mass renormalization and therefore only deal with the high-energy contributions due to correlation effects. The experimental results are compared with theoretical calculations including correlation effects using the DMFT and the 3BS schemes. In this way we obtain information on the important issue whether these state-of-the-art many-body interaction calculations cover the correlation effects in the ferromagnetic 3*d* transition metals or whether the nonlocal correlation effects not taken into account in the present calculations play an important role. Our results from SARPES experiments are compared to fully relativistic photoemission calculations within the one-step model (1SM) using the electronic structure input from DMFT and 3BS. We show that the overall results indeed establish the validity of LSDA + DMFT or 3BS many-body schemes concerning the band dispersions which get shifted closer to the Fermi energy (E_F) and also concerning satellite features in Ni. The paper is organized as follows: In Sec. II we present the experimental setup and in Sec. III we introduce the fully relativistic photoemission theory for magnetic systems. Section IV is devoted to our experimental and theoretical results. A summary is given in Sec. V.

II. EXPERIMENT

The experiments have been performed at room temperature with a hemispherical SPECS Phoibos 150 electron energy analyzer and linearly polarized undulator radiation at the UE112-PGM1 beamline at BESSY II. For spin analysis, a Rice University Mott-type spin polarimeter has been operated at 26 kV.[46] The angular resolution of the spin-resolved experiment is better than 1° and the average energy resolution about 80 meV. The Fe(110), Co(0001), and Ni(111) surfaces were prepared by epitaxial growth of 20 monolayer (ML) films on W(110) by evaporation from high purity wires using electron bombardment. The films were crystalized by postannealing during 5 min at $\sim$ 400 °C. The W(110) substrate was cleaned before deposition by several cycles of annealing in oxygen atmosphere (1×10^{-7} mbar) at 1200°C followed by flashing at 2200°C. The base pressure during the experiments was 1–2 $\times$ 10^{-10} mbar.

Figure 1(a) presents an overview of the experimental geometry. The linear polarization of the incident photon beam was horizontal or vertical, and its angle of incidence with

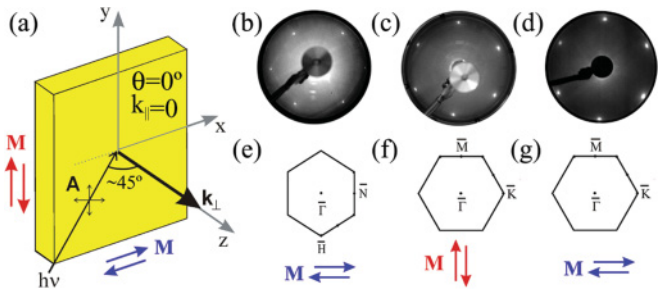

FIG. 1. (Color online) (a) Geometry of the ARPES experiment. (b) LEED pattern of the bcc Fe(011) surface. (c) Sixfold symmetry observed in the LEED pattern of the hcp Co(0001) surface. (d) LEED pattern of the fcc Ni(111) surface. (e) and (f) Sketch of the SBZs of the three surfaces. The hcp lattice is rotated by 90° with respect to the corresponding LEED pattern in (c). The magnetization orientation is also indicated in (e), (f), and (g).

respect to the surface normal ∼45° meaning that in the reference frame of the sample, the light had more p or full s character, respectively. The high structural quality of the 3d-metal films was verified by low-energy electron diffraction (LEED). Figures 1(b)–1(d) show the measured LEED patterns of the three metal surfaces acquired with an incident electron beam of ∼150 eV. Note that each diffraction spot corresponds to a $\overline{\Gamma}$ point of the corresponding surface Brillouin zone (SBZ), sketched in Figs. 1(e) and 1(f). The LEED patterns confirm that the annealing procedure which follows epitaxial growth leads to well-ordered surfaces of very high quality. In hcp Co(0001), the magnetization orientation lies out of plane in bulk single crystals[41] and in plane due to surface anisotropy effects in ultrathin epitaxial films grown on W(110).[36,47] In addition, for 20-ML-thick Fe and Ni films on W(110) the magnetization directions point in plane.[48,49] Therefore, in our experiments the samples were remantently magnetized in the film plane along the corresponding easy axis. For Fe(110) this is along $\overline{\Gamma}\,\overline{N}$, for Co(0001) along $\overline{\Gamma}\,\overline{M}$, and for Ni(111) along $\overline{\Gamma}\,\overline{K}$,[37,49–51] as indicated in Figs. 1(a), 1(e), and 1(f). The high symmetry directions along which the measurements presented in this work were performed correspond to $\mathbf{k}_\perp$ points of the bulk Brillouin zone (BBZ) going from Γ to N (Σ line), Γ to A (Δ line), and Γ to L (Λ line) for bcc Fe(110), hcp Co(0001), and fcc Ni(111), respectively. Because the emitted electrons were detected in normal emission, these high symmetry lines were probed by varying the photon energy ($h\nu$) of the incident beam in the range between 18 and 100 eV. In this geometry, the surface contribution in the SARPES signal is limited to states located at the $\overline{\Gamma}$ point of the SBZ.

III. THEORY

The photocurrent in the so-called one-step model is defined by Pendry's formula:[52]

$$I^{\mathrm{PES}} \propto \mathrm{Im}\langle \epsilon_f, \mathbf{k}_\parallel | G_2^+ \Delta G_1^+ \Delta^\dagger G_2^- | \epsilon_f, \mathbf{k}_\parallel \rangle. \tag{1}$$

The expression can be derived from Fermi's golden rule for the transition probability per unit time[53] and therefore denotes the elastic part of the photocurrent. Inelastic energy losses and corresponding quantum-mechanical interference terms[52–54] are excluded. Furthermore, the sudden approximation for the outgoing photoelectron has been applied. The photoelectron state at the detector is written as $|\epsilon_f, \mathbf{k}_\parallel\rangle$, where $\mathbf{k}_\parallel$ denotes the component of the wave vector parallel to the surface, and ϵ_f is the kinetic energy of the photoelectron. In the fully relativistic formulation $|\epsilon_f, \mathbf{k}_\parallel\rangle$ is understood as a four-component Dirac spinor. Via the advanced Green matrix G_2^- in Eq. (1) all multiple-scattering events at ϵ_f are considered and the final state can be written as $|\Psi_f\rangle = G_2^- |\epsilon_f, \mathbf{k}_\parallel\rangle$. Using the standard layer Korringa-Kohn-Rostoker (KKR) method,[55] generalized for the relativistic case,[56,57] the final state can be obtained as a time-reversed spin-polarized low-energy electron diffraction (SPLEED) state. Lifetime effects are included phenomenologically in the SPLEED calculation, by using a parametrized, weakly energy-dependent and complex inner potential $V_0(E_2) = V_{0\mathrm{r}}(E_2) + iV_{0\mathrm{i}}(E_2)$ as usual.[53,58] The real part of $V_0(E_2)$ serves as a reference energy inside the solid with respect to the vacuum level.[59] The imaginary part $iV_{0\mathrm{i}}(E_2)$, corresponds to an inelastic attenuation length of the scattered photoelectrons. To account for electronic correlations we use the LSDA + DMFT approach realized in the framework of the spin-polarized fully relativistic KKR multiple scattering theory (SPRKKR).[60] The corresponding self-energy $\Sigma^{\mathrm{DMFT}}(E)$ is calculated fully self-consistently (e.g., in charge and self-energy) from the DMFT.[17,61] Additionally we accounted for correlation effects within the 3BS approximation,[20] where the self-energy is calculated using a configuration interactionlike expansion. Due to the explicit consideration of hole and three-particle configurations this method allows for a detailed analysis of lifetime effects caused by electron-hole pair decays.

The first step in a photoemission calculation concerns the initial-state Green matrix G_1^+. This quantity is defined by the following equation,

$$[E_i - h_{\mathrm{LSDA}}(\mathbf{r})]\, G_1^+(\mathbf{r}, \mathbf{r}', E_i) = \delta(\mathbf{r} - \mathbf{r}'), \tag{2}$$

where h_{LSDA} denotes the one-particle Dirac Hamiltonian.[62,63] In atomic units ($\hbar = m = e = 1, c = 137.036$) it follows as

$$h_{\mathrm{LSDA}}(\mathbf{r}) = -ic\boldsymbol{\alpha}\boldsymbol{\nabla} + \beta c^2 - c^2 + V_{\mathrm{LSDA}}(r) + \beta\boldsymbol{\sigma}\mathbf{B}_{\mathrm{LSDA}}(r). \tag{3}$$

$V_{\mathrm{LSDA}}(r)$ denotes the (effective) spin-independent potential, and $\mathbf{B}_{\mathrm{LSDA}}(r)$ is the (effective) magnetic field given by[64]

$$V_{\mathrm{LSDA}}(r) = \tfrac{1}{2}(V^{\uparrow}_{\mathrm{LSDA}}(r) + V^{\downarrow}_{\mathrm{LSDA}}(r)), \tag{4}$$

$$\mathbf{B}_{\mathrm{LSDA}}(r) = \tfrac{1}{2}(V^{\uparrow}_{\mathrm{LSDA}}(r) - V^{\downarrow}_{\mathrm{LSDA}}(r))\,\mathbf{b}. \tag{5}$$

The constant unit vector $\mathbf{b}$ determines the spatial direction of the (uniform) magnetization as well as the spin quantization axis. β denotes the usual 4×4 Dirac matrix described in detail elsewhere.[55] G_1^+ has to be evaluated at the initial-state energy $E_i \equiv E_f - \omega$, where ω is the photon energy. To account for electronic correlations beyond the LSDA scheme one has to introduce a nonlocal, energy, and spin-dependent potential. This quantity can be defined in the following way:

$$\begin{aligned} U(\mathbf{r}, \mathbf{r}', E) = {} & \delta(\mathbf{r} - \mathbf{r}')(V_{\mathrm{LSDA}}(\mathbf{r}) + \beta\boldsymbol{\sigma}\mathbf{B}_{\mathrm{LSDA}}(\mathbf{r})) \\ & + \Sigma^{(V)}(\mathbf{r}, \mathbf{r}', E) + \beta\boldsymbol{\sigma}\,\Sigma^{(\mathbf{B})}(\mathbf{r}, \mathbf{r}', E), \end{aligned} \tag{6}$$

with

$$\Sigma^{(V)}(\mathbf{r}, \mathbf{r}', E) = \tfrac{1}{2}(\Sigma^{\uparrow}(\mathbf{r}, \mathbf{r}', E) + \Sigma^{\downarrow}(\mathbf{r}, \mathbf{r}', E)), \tag{7}$$

and

$$\Sigma^{(\mathbf{B})}(\mathbf{r},\mathbf{r}',E) = \tfrac{1}{2}(\Sigma^{\uparrow}(\mathbf{r},\mathbf{r}',E) - \Sigma^{\downarrow}(\mathbf{r},\mathbf{r}',E))\,\mathbf{b}. \quad (8)$$

The resulting integro-differential equation for the initial-state one-electron retarded Green function takes the form,

$$[E + ic\boldsymbol{\alpha}\nabla - \beta c^2 + c^2)]G_1^+(\mathbf{r},\mathbf{r}',E) + \int U(\mathbf{r},\mathbf{r}'',E)G_1^+(\mathbf{r}'',\mathbf{r}',E)d\mathbf{r}'' = \delta(\mathbf{r}-\mathbf{r}'). \quad (9)$$

According to the LSDA + DMFT approach[60] we use a self-energy $\Sigma_\alpha^{\mathrm{DMFT}}(E)$ calculated self-consistently within dynamical mean-field theory (DMFT).[61,65,66] The explicit form in relativistic notation is given by

$$U_{\Lambda\Lambda'}(\mathbf{r},\mathbf{r}',E) = [V(\mathbf{r}) + \hat{\boldsymbol{\sigma}}\,B(\mathbf{r})]\delta(\mathbf{r}-\mathbf{r}') + \Sigma_{\Lambda\Lambda'}^{\mathrm{DMFT}}(E)\delta_{l2}\delta_{l'2}. \quad (10)$$

The spin-orbit quantum number κ and magnetic quantum number μ are combined in the symbol $\Lambda = (\kappa,\mu)$. In the current fully relativistic implementation the perturbative SPTF solver (spin-polarized T matrix + FLEX)[67] is used. For an explicit photoemission analysis the single-site scattering t matrix of an atomic potential and the corresponding wave functions are directly imported from the electronic structure calculation. Consequently, the photoemission calculation is no longer restricted to the single-particle DFT Hamiltonian [Eq. (3)] because the relevant physical quantities connected with the initial-state Green matrix and used for spectroscopical analysis, as, for example, the matrix elements or the single-site scattering matrix contain the electronic correlations beyond the LSDA scheme. The remaining restrictions are mainly due to the SPTF solver and are due to the fact that our self-energy is a local quantity. In principle, both types of restrictions can be removed, the first one by using a quantum Monte Carlo type solver, the second one by applying for example a cluster-DMFT approach.

IV. RESULTS AND DISCUSSION

A. Spin and angle-resolved photoemission from Fe, Co, and Ni

Figure 2 shows a comparison between the spin-integrated experimental spectra [Figs. 2(a)–2(c)] and the corresponding theoretical LSDA + DMFT + 1SM calculations [Figs. 2(d)–2(f)] of bcc Fe(110), hcp Co(0001), and fcc Ni(111), respectively, obtained for p-polarized photons and along the different directions of the BBZ mentioned above. In Fig. 3, similar data to the ones presented in Fig. 2 are shown, for both experiment [Figs. 3(a)–3(c)] and calculations [Figs. 3(d)–3(f)], but now at a few selected photon energies and spin resolved. The **k** values were calculated from the measured photon energies by using the inner potentials $V_0(\mathrm{Fe}) = 14.5$ eV, $V_0(\mathrm{Co}) = 14.8$ eV, and $V_0(\mathrm{Ni}) = 13.4$ eV.

To find the best correspondence between the BE positions of the experimental and theoretical peaks we have used for the averaged on-site Coulomb interaction U the values $U(\mathrm{Fe}) = 1.5$ eV, $U(\mathrm{Co}) = 2.5$ eV, and $U(\mathrm{Ni}) = 2.8$ eV. For Fe, the adopted U value is within the experimental value $U \sim 1$ eV[32] and a value $U \sim 2$ eV derived from theoretical studies.[68,69] In the case of Co and Ni the U values are in agreement with previous theoretical and experimental investigations.[24,39,43]

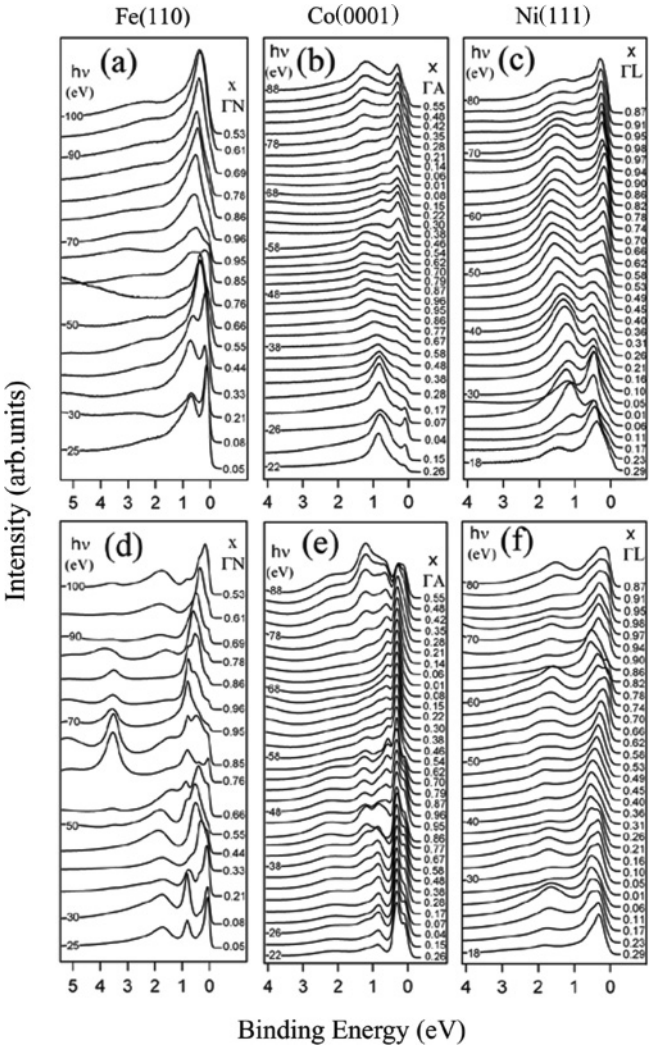

FIG. 2. (Upper panel) Series of experimental spin-integrated photoemission spectra of (a) bcc Fe(110), (b) hcp Co(0001), and (c) fcc Ni(111) measured with p polarization in normal emission along the ΓN, ΓA, and ΓL directions of the corresponding BBZ at different excitation energies in steps of 2 eV. On the left, several photon energies are given. On the right, the curves are labeled by the wave vectors in units of Å^{-1}. (Lower panel) (d) and (e) Corresponding calculations obtained by the LSDA + DMFT + 1SM method for an in-plane magnetization according to the experimental situation.

Because the screening of the exchange interaction is usually small, the averaged on-site interaction J is generally accepted to coincide with its atomic value which is approximately equal to $J \sim 0.9$ eV for all $3d$ elements and can be directly calculated.[70] Therefore, unless specified, these have been the U and J values used in most of the calculations presented here. Starting with these parameters and from a detailed comparison between theory and experiment such as the one presented in Figs. 2 and 3, we were able to identify the nature of different transitions appearing in the theoretical and experimental spectra. For Fe and Co, a detailed analysis of this type has been carried out elsewhere.[31,40] It is important to remark that our study is focused on the energy range $0.2 \leqslant \mathrm{BE} \leqslant 2.5$ eV where renormalization effects are predominantly caused by

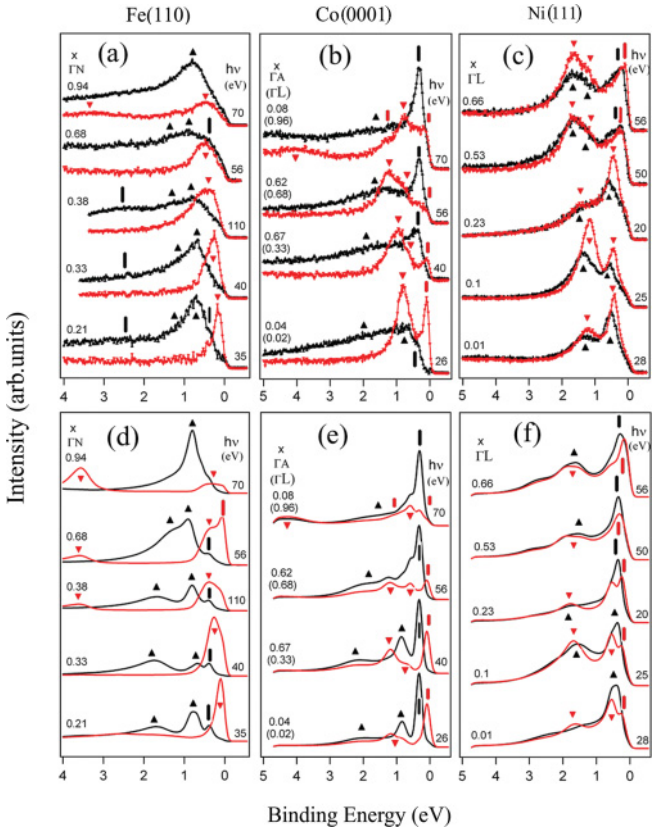

FIG. 3. (Color online) Analogous data as in Figs. 1(a)–1(f) but now spin resolved. (Upper panel) Experiment [upward black (dark) triangles, majority spin states; downward red (light) triangles, minority spin states). (Lower panel) (d)–(f) LSDA + DMFT + 1SM theory [black (dark) and red (light) lines for majority and minority spin electrons, respectively]. Additional labels on top of the spectra indicate majority [black (dark) triangles] and minority [red (light) triangles] bulk states, while vertical black (dark) [red (light)] bars majority [minority] spin surface-related features. The curves are labeled by the photon energies (right) and the wave vectors (left) for all lattices in units of Å^{-1} for comparison.

electron-hole excitations with and without spin flips. This energy range is quite different from that discussed in recent high-resolution ARPES studies on Fe or Ni.[28,30,71] There, the very low BE range $E_B \leqslant 300$ meV has been treated, in which a renormalization of the charge carrier dynamics by a coupling to phonon or magnetic excitations is important. All the observed peaks in Figs. 2 and 3 correspond to majority (↑) and minority (↓) spin states of different symmetries. They are due to direct interband transitions from t_{2g} and e_g bulk states which change their initial energy as $h\nu$ varies, as well as surface emission peaks and resonant structures. For Fe and Ni, we will describe the symmetries of these states following the nonrelativistic notation described by Hermanson for bcc and fcc crystals,[72] respectively. For Co, the simpler relativistic notation given by Benbow[73] for hcp crystals will be used.

Closest to the Γ point, the Fe experimental spectra [Figs. 2(a) and 3(a)] and the corresponding LSDA + DMFT + 1SM calculations [Figs. 2(d) and 3(d)] exhibit an intense peak close to E_F which we attribute to a $\Sigma_{1,3}^{\downarrow}$ minority spin surface resonance. In agreement with the theoretical results, its $\Sigma_3^{\downarrow}$ bulk component crosses E_F at $x \sim 0.33$ ΓN, leading to a strong reduction of the intensity in the minority spin channel starting from values around $x = 0.68$ ΓN. The next Fe peak at a BE of ∼0.7 eV, visible in both theory and experiment in a large range of wave vectors between Γ and N, can be assigned to almost degenerate $\Sigma_{1,4}^{\uparrow}$ bulklike majority spin states. Other peaks at higher BE, such as the broad feature around a BE of ∼2.2 eV, visible at various **k** points but not at the N point, is related to a majority $\Sigma_{1,3}^{\uparrow}$ surface resonance[31] (we will come back to this discussion in Secs. IV B and IV D). Around the N point and at a BE $\geqslant 3$ eV, a $\Sigma_1^{\downarrow}$ band having strong sp character can also be observed. Note that the background intensity of the experimental spectrum at $x = 0.66$ ΓN ($h\nu = 55$ eV) is strongly increasing due to the appearance of the Fe $3p$ resonant structure. We emphasize that in the present calculations additional lifetime effects for the sp bands and resonant-photoemission processes above the resonance threshold such as Auger electron emission are not considered.

For Co, the comparison between experiment [Figs. 2(b) and 3(b)] and theory [Figs. 2(e) and 3(e)] reveals that all the peaks appearing near E_F in the full $h\nu$ range and for a BE lower than ∼0.5 eV can be attributed to the two majority and minority spin counterparts of a Tamm-like surface feature.[38] The minority spin component of this state located at a BE of $E_B \sim 0.05$ eV lies within the gap appearing around E_F and it can be identified as a pure surface state of $\Delta_9^{\downarrow}$ symmetry. Its majority spin counterpart appears as a nondispersing feature in the full $h\nu$ range at a BE of ∼0.4 eV. It can be identified as a surface resonance feature of $\Delta_{9,7}^{\uparrow}$ symmetry because it is located at the border of the gap and almost degenerate with the $\Delta_{9,8}^{\uparrow}$ majority bulk bands appearing near the same BE. In the calculations, however, it exhibits a significantly narrower linewidth at all photon energies and much stronger intensity in a $h\nu$ range between 26 and 38 eV ($0.04 \leqslant x \leqslant 0.58$). In addition, at the Γ point ($x \sim 0.08$ ΓA, $h\nu = 26$ eV) it is seen in the experiment as a majority spin shoulder close to E_F, but in the theoretical spectra as a sharp and intense feature. We attribute this deviation to a theoretical underestimation of the multiple scattering events occurring between surface and bulk electron wave functions. On the other hand, all the Co bands at a higher BE than ∼0.5 eV and in the complete Co BBZ are bulklike. Besides the almost degenerate and relatively narrow bulk minority spin bands located in a BE range between ∼0.8 eV and ∼1.2 eV, we observe much broader majority spin bulklike states of $\Delta_9^{\uparrow}$ and $\Delta_7^{\uparrow}$ symmetries in a BE range from about ∼1.4 eV to ∼1.9 eV. In the experiment, these states are best resolved in Fig. 3(b) at $x = 0.67$ ΓA ($h\nu = 40$ eV) and $x = 0.62$ ΓA ($h\nu = 56$ eV). In the calculations they appear more pronounced in intensity but their BE is approximately reproduced. Only peaks with strong sp character are observed at BE energies higher than 2 eV, such as the minority spin sp band of $\Delta_8^{\downarrow}$ symmetry appearing at $k \sim 0.08$ ΓA ($h\nu = 70$ eV) in Fig. 3(b) and at a BE of about 4.3 eV. Note that in the calculated spectrum of Fig. 3(e), the sp band in Co appears somehow broadened as compared to what was found in the Fe calculations. Considering that no corrections due to electronic correlations have been applied to the *sp* states, we explain this

by the intrinsic differences in initial and final-state dispersions of these bands.

In the case of Ni, the photoemission signal in both experiment [Figs. 2(c) and 3(c)] and theory [Figs. 2(f) and 3(f)] contains a prominent contribution from bulk states of Λ_3 and $\Lambda_{1,3}$ symmetries. In addition to these states, *d*-band and *sp*-derived surface states relatively mimicked under bulk emission contribute to the spectra as well. Closest to E_F and at a BE of ∼0.2 eV, we identify the contribution from a *sp*-like Λ_3 surface state, in agreement with previous studies.[74] For photon energies below $h\nu = 46$ eV, this state appears as a single shoulder in both theory and experiment while at higher photon energies it can be distinguished as a sharp feature. It strongly overlaps with the bulk bands of the same symmetry leading to an intense surface resonance structure in almost the complete Ni BBZ. Due to the limited energy resolution, contributions closer to E_F, from the Shockley surface state which is also well known for other nonmagnetic fcc (111) surfaces[75] and which is reproduced in our LSDA + DMFT + 1SM calculations slightly above E_F, are not observable in our experiments. On the other hand, at a BE of ∼1.2 eV we do observe the minor contribution of a second *d*-band-derived surface state. This state appears as a shoulder in the experiment and is best resolved in almost the complete Ni BBZ at photon energies larger than ∼32 eV. Also in the calculations, it strongly overlaps with the bulklike bands of Λ_1 and Λ_3 symmetries around the same BE, leading to surface-resonance-enhanced bulklike states that are degenerate at the Γ point and exhibit a relatively small dispersion when moving toward the L point.

Concerning the quality of the agreement between the theoretical and experimental spectra shown in Figs. 2 and 3, up to some extent we find good agreement for most of the BE positions of the different peaks. However, in the case of Fe a more detailed examination of the experimental spectra reveal a shoulder which is located at the higher BE side of the bulk $\Sigma^{\uparrow}_{1,4}$ peak at a BE around ∼1.2 eV and most visible in Fig. 3(a) for $0.33 \leqslant x \leqslant 0.68$ and which is not reproduced in the calculations. This state can be well resolved with *s*-polarized photons (for more details see Sec. IV D). We have previously shown that it can be assigned to a bulklike $\Sigma^{\uparrow}_{1,3}$ state[31] and as we will discuss later this opens up the question whether for Fe correlation effects in the present calculations using $U = 1.5$ eV are underestimated and a stronger band narrowing is needed to achieve better agreement between theory and experiment (see Sec. IV D). For Co, on the other hand, we emphasize that we do not observe majority spin quasiparticle bands at a BE higher than ∼2 eV. This is in contrast to recent experimental conclusions,[41] where most probably high-energy tails in the ARPES spectrum were identified as quasiparticle peaks at a BE ∼ 3 eV. Because our finding is in agreement with a previous theoretical analysis in the framework of the 3BS theory,[39] we explain this by the quenching of the majority spin channel quasiparticle excitations in this system. In Ni, this effect is less pronounced because the band narrowing is larger than in Co. Finally, concerning the linewidths, we observe a larger broadening of the experimental peaks indicating that the theory underestimates the scattering rates. We emphasize that this is a general feature in all Fe, Co, and Ni calculations presented here.

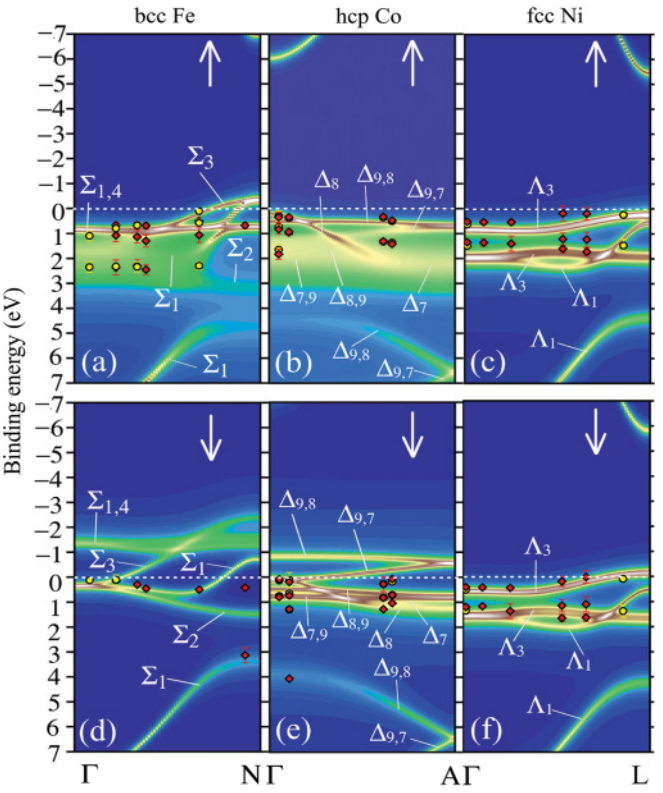

FIG. 4. (Color online) Bloch spectral functions of bcc Fe(110), hcp Co(0001), and fcc Ni(111). The photoemission peak positions are obtained from spin-resolved measurements for different polarizations (diamond for *p* and circle for *s* polarization). The spin-projected Bloch spectral functions are obtained by the LSDA + DMFT method for majority (upper panel) and minority (lower panel) spin states. The symmetries of the different states are also indicated.

B. Many-body effects in the spin-dependent bulk band structures of Fe, Co, and Ni

In order to further examine all the many-body aspects of the band structures of Fe, Co, and Ni, in Fig. 4 we compare the BE positions of the different experimental peaks appearing in the SARPES spectra to the calculated bulklike spin-dependent spectral functions $A(\mathbf{k},E)$ obtained from the LDSA + DMFT method. Figures 4(a) and 4(d) present the Fe results, Figs. 4(b) and 4(e) the Co spectral functions, and Figs. 4(c) and 4(f) show the results for Ni, each spectral function with the corresponding symmetry labels. Majority spin states are shown in Figs. 4(a)–4(c) and minority spin states in Figs. 4(d)–4(f). Due to the neglection of matrix element effects in the calculations the complete spin-resolved bulk band structure is visible in each case. The experimental peak positions were extracted by accurately fitting the measured SARPES data (see Sec. IV D) of Figs. 3(a)–3(c) for *p* polarization and similar SARPES data for *s* polarization (not shown). The fitted BE positions resulting from this procedure are indicated by red diamonds and yellow circles for *p* and *s* polarization, respectively. The majority spin spectral functions shown in Figs. 4(a)–4(c) reproduce the experimental data with an overall better agreement than the well-known peak positions from standard LSDA calculations.[24,40,43] Majority spin states

exhibit pronounced shifts of the 3*d*-band complex toward E_F and a significantly reduced 3*d*-band width again in all three cases when compared to the LSDA results. These two facts indicate that a shrinking of the 3*d* bands due to correlation effects are necessary to properly describe the experimental data. This is clearly demonstrated for Co and Ni in Figs. 4(b) and 4(c), where a relatively good agreement is obtained for the BE positions of the experimental majority spin peaks, in agreement with the results presented in Figs. 3(b) and 3(c). Slight deviations between experiment and theory appear for the Ni majority bands which are located relatively close to E_F. The experimental peaks show up at ∼0.2 eV lower binding energies. This fact can be explained in terms of sp-like surface emission which is quite strong in Ni but not considered in the bulklike spectral function. These deviations are less pronounced in the comparison between experiment and LSDA + DMFT + 1SM calculations because within the 1SM surface emission is quantitatively taken into account. For Fe, by comparing the experimental peak positions with the calculated spectral function shown in Fig. 4(a), we obtain for binding energies close to E_F good agreement for most of the peak positions. On the other hand, the situation appears different for higher binding energies, especially near the Γ point. The experimental peak position at about ∼2.2 eV can be reproduced by plain LSDA calculations (see Sec. IV D) but completely neglecting correlation effects in Fe would make the overall comparison between theory and experiment much worse, in particular at binding energies smaller than ∼1.5 eV. Thus, as mentioned in the previous subsection, we have assigned this experimental peak position to a surface feature.[31]

Inspecting Figs. 4(d)–4(f) which are related to the minority spin systems for Fe, Co, and Ni, we observe that the experimental peak positions are more or less reproduced by the calculated LSDA + DMFT band dispersions. For Co only the $\Delta_9^{\downarrow}$ minority spin component of the Tamm state that appears halfway between Γ and A in the vicinity of E_F is not visible in the bulklike calculational results, as expected. The same happens for Fe near the *N* point. In contrast to majority spin states, it is well established that LSDA + DMFT and LSDA spectral function calculations for minority spin states[24,40,43] exhibit minor differences, meaning that the BE positions of the different bands in the two LSDA and LSDA + DMFT theoretical approaches show relatively good agreement with the experimental data. This can be explained by the fact that correlation effects are much less pronounced in the minority spin channel. The explanation for reduced correlation effects can be found in terms of electron-hole pair creation in the minority spin channel. Since Fe, Co, and Ni have more empty minority than majority spin states for any processes involving electron-hole pair creation, the pair is more likely to appear in the minority spin bands. This means that any scattering process involving majority spin electrons mostly leads to the creation of minority spin electron-hole pairs determined by *U*. Scattering processes involving minority spin electrons also lead to the creation of minority spin electron-hole pairs, but the effective interaction for parallel-spin pairs is determined by *U*-*J* < U. Therefore, for moderate *U* values correlation effects are stronger for majority spin electrons.

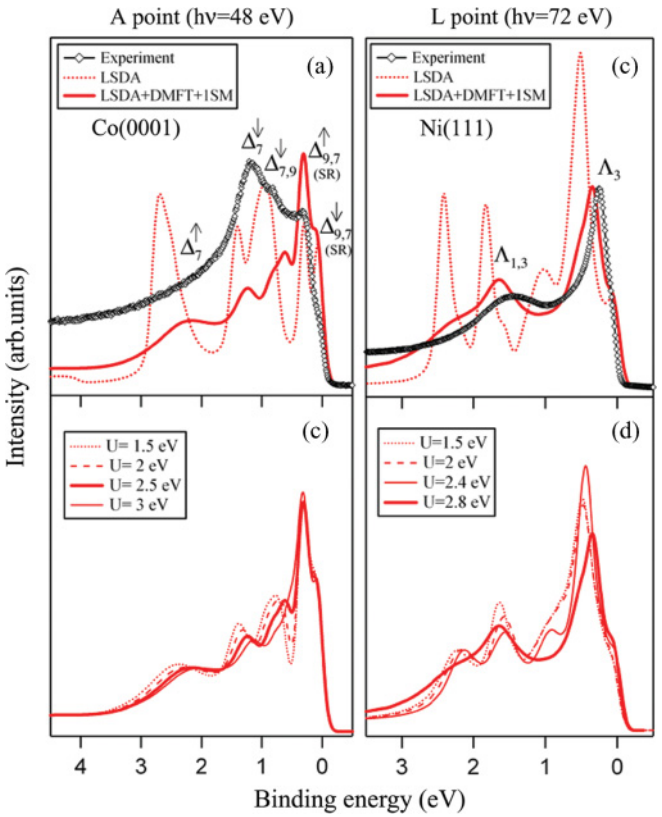

FIG. 5. (Color online) Comparison between experimental and theoretical spectra at the *A* point of Co(0001) [(a) and (b) ($h\nu$ = 48 eV)] and at the L point of Ni(111) [(c) and (d) ($h\nu$ = 72 eV)] for *p* polarization. (a and c) Spin-integrated experimental spectra [thick black (dark) dots], single-particle LSDA-based calculation including surface effects [thick dotted red (light) line] and LSDA + DMFT + 1SM spectra [thick solid red (light) line]. (b and d) Spin-integrated LSDA + DMFT + 1SM calculations for different *U* values. Thin red (light) dotted, dashed, thick, and thin solid lines for *U* = 1.5, 2, 2.5, and 3 (2.8) eV, respectively. In (a) and (c), symmetry labels in the two corresponding BBZ are also indicated.

Let us now focus on the agreement between the experimental and theoretical LSDA + DMFT + 1SM spectra for Ni and Co as a function of the on-site Coulomb interaction *U*, as shown in Fig. 5. Similar results for Fe will be shown in Sec. IV D. We emphasize that *U* is the only parameter which might lead to important changes in the calculated SARPES spectra. Because the relatively small exchange parameter *J* = 0.9 eV is only weakly screened, the small changes in *J* do not lead to significant differences in our calculations on the energy scale we are focusing on. This is due to our construction of the many-body computational schemes, and in particular due to the fact that double counting terms in our DMFT and 3BS simulations are obtained from LSDA spin-polarized solutions.

Figures 5(a) and 5(b) compare spin-integrated experimental spectra near the edge of the BBZ of Co and Ni to LSDA + DMFT + 1SM and LSDA calculations broadened by the experimental energy resolution. Figures 5(b) and 5(d) include the corresponding spin-dependent LSDA + DMFT + 1SM calculations for *U* ranging from 1.5 to ∼3 eV. Figure 5(a) shows this comparison at the A point of Co (x = 0.96 ΓA, $h\nu$ = 48 eV) and Fig. 5(b) at the L point

of Ni ($x = 0.97$ ΓL, $h\nu = 72$ eV). The LSDA calculations include surface effects for a clear comparison. The spin character and symmetry of the different experimental states are also given. Both the Co and Ni LSDA + DMFT + 1SM calculations lead to an important improvement as compared to the LSDA calculations. We see that by including spin-dependent electron correlations, the BE positions of the theoretical peaks agree relatively well with the experimental ones.

Regarding Co majority and minority spin states near the Fermi level, in Fig. 5(a) a good agreement is achieved for the BE positions of the $\Delta^{\uparrow}_{9,7}$ and $\Delta^{\downarrow}_{9,7}$ surface resonances in both the LSDA + DMFT + 1SM and LSDA calculations. The $\Delta^{\downarrow}_{7,9}$ minority spin bulklike state, on the other hand, is shifted to a BE of $E_B \sim 0.79$ eV in the experiment and to $E_B \sim 0.63$ eV in the LSDA + DMFT + 1SM calculation with respect to the LSDA value of $E_B \sim 0.96$ eV. At higher BE, the $\Delta^{\downarrow}_{7}$ peak appears in the experiment at $E_B \sim 1.17$ eV while in the LSDA + DMFT + 1SM calculation at $E_B \sim 1.22$ eV, compared to a value of $E_B \sim 1.4$ eV in the LSDA calculation. Previously, we have done a similar analysis in the whole Co BBZ by checking in detail the differences between experiment and LSDA spectral function calculations.[40] We find that these differences can be explained with a linear variation of the self-energy according to $\mathrm{Re}\Sigma \approx 0.27\ E$ corresponding to an averaged mass enhancement of $m^*/m_0 \approx 1.27$ for majority spin states which is the closest we obtain to the theoretical value of $m^*/m_0 \approx 1.31$ for $U = 2.5$ eV, where m_0 is the bare-particle mass. For Ni states shown in Fig. 5(b), near E_F the Λ_3 surface resonance appears in the experiment at $E_B \sim 0.2$ eV and is shifted to $E_B \sim 0.3$ eV in the LSDA + DMFT + 1SM calculation with respect to a BE of $E_B \sim 0.5$ eV in the LSDA approach. The second $\Lambda_{1,3}$ surface resonance at a higher BE is also shifted in the experiment to $E_B \sim 1.3$ eV and to $E_B \sim 1.6$ eV in the LSDA + DMFT + 1SM calculation compared to LSDA where it appears at a BE of $E_B \sim 2.41$ eV. Furthermore, we have compared in detail the experimental peak positions with Ni LSDA peak position calculations at different photon energies (not shown). Our results are consistent with an averaged experimental mass enhancement of $m^*/m_0 \approx 1.9$ which should be compared to the theoretical value of $m^*/m_0 \approx 1.8$ which we obtain for $U = 2.8$ eV. The calculated mass enhancement is largest in Ni and consistent with a reduction in the bandwidth of majority spin states of about ∼50% due to correlation effects, while effects in the minority spin channel are only minor. In contrast, the reduction in the bandwidth of ∼37% obtained for Co majority spin states leads to a smaller mass renormalization, indicating that correlation effects are weaker in Co than in Ni.

We emphasize that for different U values an identical analysis can be carried out by extracting the BE positions of the different peaks appearing in Figs. 5(b) and 5(d), but also from a more general comparison of the experimental and LSDA + DMFT peak positions with the LSDA spectral function calculations. In general, we estimate that the deviations between the experimental and theoretical mass enhancement factors for different U values are not large, at least in the window of U values used in the calculations. Nevertheless, from our analysis we conclude that $U = 2.5$ eV for Co and $U = 2.8$ eV for Ni lead to best agreement with experiments. It is important to remark that a precise determination of U requires an analysis of this type at various $\mathbf{k}_\perp$ points of the BBZ, from which we achieve similar conclusions. We emphasize that in our simulations U and J are not exactly treated as totally free parameters in order to fit the experimental data. In fact the window of accessible values for both of them can be obtained by combining *ab initio* simulations with different techniques.[76]

TABLE I. Values of the experimental and theoretical mass enhancement factors m^*/m_0 for majority spin states at high symmetry points of the BBZ of Fe, Co, and Ni, respectively. The theoretical values are derived for U(Fe) = 1.5 eV, U(Co) = 2.5 eV, U(Ni) = 2.8 eV.

Fe			Co			Ni		
	Expt.	Theory		Expt.	Theory		Expt.	Theory
Γ	1.7	1.2	Γ	1.26	1.31	Γ	2.0	1.8
N	1.1	1.2	A	1.29	1.31	Λ	1.9	1.8

We also notice that in Figs. 5(b) and 5(d) increasing the value of U does not shift the peaks significantly toward E_F. This can be attributed mainly to the fact that there are no strong changes in Σ_{DMFT} in a region very close to E_F and to the existence of surface-related features which in our calculations are not strongly sensitive to changes in the U parameter. In addition, due to the hexagonal structure in Co most of the bulk bands are located in a narrow energy interval and exhibit a weak bulk-surface coupling while in Ni the coupling between surface and bulk states is stronger and extends to higher BE energy.

In Table I, we summarize the experimental and theoretical majority spin mass enhancement factors obtained for Fe, Co, and Ni at high symmetry points of the BBZ. For Fe, at the Γ point (see Sec. IV D for details), the difference between experiment and LSDA calculations can be explained with a linear variation of the self-energy according to $\mathrm{Re}\Sigma \approx 0.7\ E$ corresponding to a mass enhancement $m^*/m_0 \approx 1.7$. This should be contrasted to the theoretical value of $m^*/m_0 \approx 1.2$ obtained for $U = 1.5$ eV in the present work. However, at the N point, we obtain a reduced value of $m^*/m_0 \approx 1.1$ leading to a more satisfactory agreement. This result is closely related to a previous ARPES study,[28] where close to E_F differing mass renormalizations have been detected at various high symmetry points of the Fe BBZ. These differences could indicate a strong influence of nonlocal correlation effects in the case of Fe.[31] However, we emphasize that nonlocal correlations are not considered in the present calculations because the self-energy is seen as a local quantity, as discussed in Sec. III.

C. Satellite features: Ni

The electronic structure of fcc Ni has been the subject of numerous experimental[77–84] and theoretical studies[85–87] as a prototype of an itinerant electron ferromagnet, since shortcomings of simple one-electron theory are obvious. As discussed above, LSDA calculations for fcc Ni cannot reproduce various features of the electronic structure of Ni which had been observed experimentally. Besides the fact

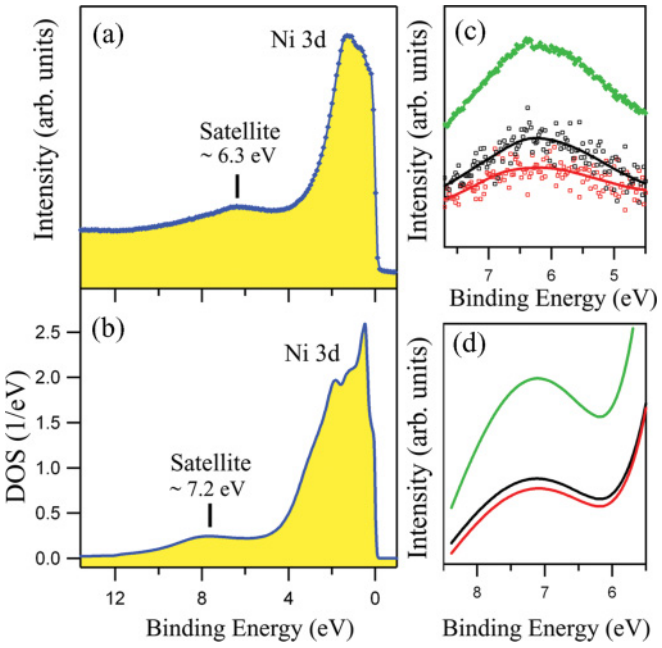

FIG. 6. (Color online) (a) Experimental Ni angle-integrated photoemission spectrum taken at $h\nu = 150$ eV. The Ni 6-eV satellite structure appears at about 6.3-eV binding energy. (b) LSDA + DMFT calculation of the spin-integrated DOS for a U value of 2.8 eV. The satellite feature appears at about 7.2-eV binding energy. (c) Spin- and angle-resolved photoemission spectra taken in normal emission at $h\nu = 66$ eV with s-polarized light. Open black (dark) squares, majority spin states; open red (light) squares, minority spin states; solid black (dark) and red (light) lines serve as guides for the eyes. Spin-integrated intensity, green (gray) thick dotted line. (d) LSDA + DMFT + 1SM spin-resolved photoemission calculation in normal emission at $h\nu = 66$ eV for a U value of 2.8 eV; solid black (dark) and red (light) lines indicate majority and minority spin states; green line shows the spin-integrated intensity.

that valence band photoemission spectra of Ni[21–23] show a reduced 3d-band width compared to LSDA calculations[88] the spectra show a dispersionless feature at a BE of about 6 eV, the so-called 6-eV satellite,[77,78,89–92] which is not reproducible within the LSDA approach. On the other hand, an improved description of correlation effects for the 3d electrons using many-body techniques[19,85,86] or in a more modern view applying the LSDA + DMFT scheme[24,60,93] results more or less in the experimental width of the 3d-band complex and furthermore is able to reproduce the 6-eV satellite structure in the valence band region. As was shown by earlier calculations[19] and was confirmed by photoemission experiments,[91] the 6-eV satellite is spin polarized. In our experimental study we measured the Ni angle-integrated photoemission intensity at $h\nu = 150$ eV but also measured SARPES spectra at $h\nu = 66$ eV with s-polarized photons. Corresponding results are shown in Figs. 6(a) and 6(c). The satellite feature is clearly visible in both measurements at a BE of about 6.3 eV fully in agreement with all former investigations.[91,92] Furthermore, Fig. 6(c) shows the spin polarization of the satellite in the spin-resolved experiment, again in full agreement with earlier studies.[91] After background substraction, the spin polarization amounts to about 15%. In Fig. 6(b) we compare the experimental results with a DOS calculation which is based on the LSDA + DMFT approach. The parametrization for $U = 2.8$ eV and $J = 0.9$ eV is identical with the values which we used for the SARPES calculations. The satellite appears at a BE of ~7.2 eV. This is about 1 eV higher in BE when compared to the experimental result. The explanation for this is found in terms of the many-body solver. The so-called FLEX solver[67] is of perturbative nature compared to a quantum Monte Carlo solver which is able to consider the complete diagrammatic expansion of the self-energy in a statistical way. As a consequence the energy dependence of the self-energy is less pronounced and this causes the observed shift of about 1 eV in the BE. Nevertheless, the satellite is observable in the calculated DOS and therefore one would expect its appearance in the theoretical photoemission intensity as well. The corresponding spin- and angle-resolved photoemission calculation is shown in Fig. 6(d). The green color shows the spin-integrated intensity, whereas the black (dark) and red (light) lines indicate the majority and minority spin-related intensities. The satellite structure is present at a BE of ~7.2 eV and the calculated spin polarization amounts to about 10% which is slightly smaller than the experimental one. Besides these small deviations between experiment and theory, the agreement at which we show the first angle-resolved photoemission calculation for Ni metal in which this spectral feature appears is very satisfying.

D. Spin-dependent quasiparticle lifetimes: a comparison between Fe, Co, and Ni

Finally we want to discuss the level of agreement between the experimental and theoretical linewidths obtained for the different Fe, Co, and Ni photoemission peaks. Our previous SARPES studies indicated that the photoemission calculations in general underestimate the scattering rates.[31,40] First of all we will concentrate on Fe again, because from the data shown in Figs. 1–3 we find indications that nonlocal correlation effects are most pronounced in this system, as mentioned above. Figure 7 demonstrates this for data close to the Γ point ($k = 0.05$ ΓN). In Fig. 7(b) we compare the experimental data obtained for p-polarized light with LSDA calculations broadened with the experimental energy resolution, with a LSDA + DMFT calculation and with a LSDA + DMFT + 1SM calculation. At low BE we achieve good agreement for the minority $\Sigma^{\downarrow}_{1,3}$ surface resonance. For the bulk $\Sigma^{\uparrow}_{1,4}$ peak at BE of ~0.65 eV, the deviations are more pronounced. This holds also for the $\Sigma^{\uparrow}_{1,3}$ peak which appears in the LSDA calculation at a BE of ~2.2 eV. Using a U value of 1.5 eV in the LSDA + DMFT + 1SM calculation the agreement is slightly improved. This is clearly observable from Fig. 7(a) in which we compare spin-resolved spectra obtained for s polarization with the corresponding experimental data. Due to the correlation correction via LSDA + DMFT the $\Sigma^{\uparrow}_{1,3}$ peak shifts to a lower BE of ~1.5 eV and the peak classified before from the LSDA calculation as bulk $\Sigma^{\uparrow}_{1,3}$ is now identified as a $\Sigma^{\uparrow}_{1,3}$ surface resonance in agreement with experiment. The bulklike $\Sigma^{\uparrow}_{1,4}$ peak only visible for p-polarized light also shifts slightly in energy but again the shift is too small by using $U = 1.5$ eV. This is indicated in the experimental

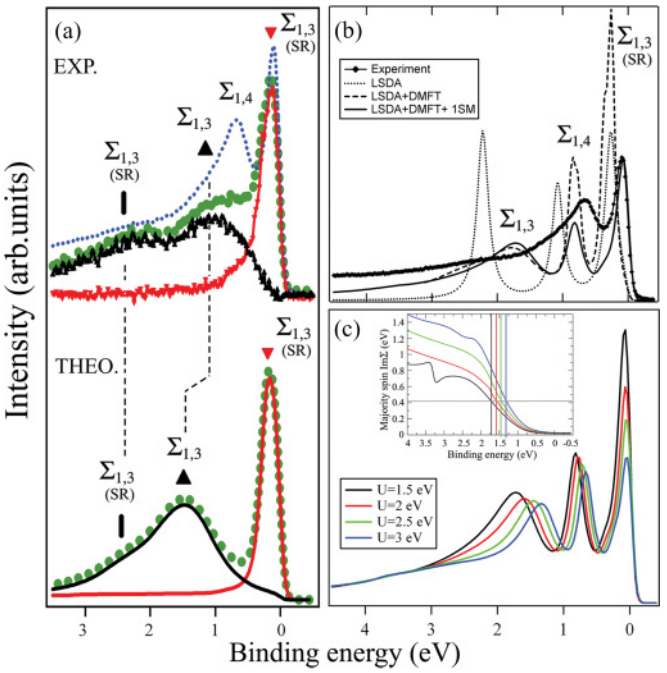

FIG. 7. (Color online) (a) Comparison of spin-resolved experimental spectra near the Γ point (top) obtained for *s*-polarized light with corresponding photoemission calculations using a U value of 1.5 eV (bottom). Blue (gray) thin dotted line, experimental spin-integrated spectrum obtained for p polarization; black (dark) upward triangles and solid lines, majority spin states; red (light) downward triangles and solid lines, minority spin states; green (gray) thick dotted line, spin-integrated intensity. (b) Comparison between the spin-integrated experimental spectra of Fe(110) at the Γ point for p polarization with the single-particle LSDA-based calculation, the LSDA + DMFT spectra, and the LSDA + DMFT + 1SM spectra. (c) LSDA + DMFT + 1SM calculations for $U = 1.5$–3 eV. The inset shows the energy dependence of $\mathrm{Im}\Sigma_{\mathrm{DMFT}}$ for U values from 1.5 to 3 eV.

part of Fig. 7(a) by the blue dotted line which represents the spin-integrated spectrum obtained for p polarization. From this comparison, as already mentioned in Sec. IV A the appearance of a shoulder in the p-polarization data due to the $\Sigma^{\uparrow}_{1,3}$ band which is also visible in Fig. 3(a) can be clearly observed. Thus we may conclude that correlation effects in the present calculations are underestimated using $U = 1.5$ eV and that a stronger band narrowing is needed. In Fig. 7(c) a series of U-dependent LSDA + DMFT + 1SM photoemission spectra is shown to further clarify this. The black (dark) solid line represents the spectroscopical calculation for $U = 1.5$ eV that is also shown in Fig. 7(b). Figure 7(c) reveals that a U value of about 3 eV is necessary to better reproduce all the experimental peak positions for **k** values close to the Γ point. On the other hand, to predict such high U values for all **k** points in the BBZ is unrealistic, considering that a variety of binding energies exist for certain **k** points where lower U values would be the best option.[31] Moreover, such high U values are outside the previously mentioned range of $U \sim$ 1–2 eV, and in addition, we still are left with the problem that the calculated linewidths are far too small compared with the experimental ones. Furthermore, the real part of the self-energy is closely connected with the imaginary part by the Kramers-Kronig relations. A relatively small constant U value results in a relatively weak energy dependence of the real part of Σ and via the Kramers-Kronig relations causes a relatively weak energy dependence of the corresponding imaginary part. The imaginary part itself controls the linewidths of the photoemission peaks which should be comparable for experiment and theory. However, we find that the calculated linewidths in most but not all cases are too small in comparison with the experimental data. In this context one has to discuss the remarkable fact that in the BE window of interest, in the present calculations the linewidth has the general property of not increasing with increasing U [see Fig. 7(c)]. This can be explained in terms of the energy dependence of ImΣ and by the fact that with increasing U the peak positions move to lower binding energies leading to an almost constant ImΣ. This effect is visualized in the inset of Fig. 7(c) which shows the calculated majority spin $\mathrm{Im}\Sigma_{\mathrm{DMFT}}$ for different U values, where vertical lines indicate the BE energy shift of the $\Sigma^{\uparrow}_{1,3}$ majority spin bands as an example. While $\mathrm{Im}\Sigma_{\mathrm{DMFT}}$ increases because correlation effects are stronger for larger U values, the horizontal gray line demonstrates that the width of these peaks does not increase with increasing U. With U-dependent peak BE positions of 1.72 eV ($U = 1.5$ eV), 1.60 eV ($U = 2$ eV), 1.45 eV ($U = 2.5$ eV), and 1.32 eV ($U = 3$ eV) a majority spin $\mathrm{Im}\Sigma_{\mathrm{DMFT}} = 0.42$ eV is obtained, which means that the lifetime around the peak maxima of the $\Sigma^{\uparrow}_{1,3}$ bands is nearly identical for all U values. This is a general feature of all the peaks appearing in the spectra. This fact gives further indication that for the linewidths not only the strength of an averaged U value is of major importance but also the self-energy as a function of the energy E itself. In this sense we expect a strong variation of U as a function of E and **k** by introducing a nonlocal U which results not only in a **k**-dependent self-energy but also affects the dependence of Σ as a function of E.

With the help of a fitting procedure we have extracted the experimental peak positions shown in Figs. 3(a)–3(c) and obtained more quantitative information on the discrepancies between experimental and theoretical linewidths. The use of spin resolution is crucial in this case because the calculated self-energy is spin dependent and we expect the experimental linewidths of the initial states to be spin dependent as well. The experimental spin-resolved spectra were fitted at several **k** values by a sum of Lorentzians plus a background. The fitting procedure has been described in more detail elsewhere.[40] For a particular **k** point, a typical SARPES spectrum containing N peaks is fitted by a function involving a convolution of the form:

$$I_k^{\uparrow,\downarrow}(E) = \left[f(E,T) \sum_{i=1}^{N} M_i^2 A_{k\,i}(E_i,\omega_i) + B_k(E) \right] \otimes G(h\nu), \tag{11}$$

where E_i, ω_i, and the matrix elements M_i are fitting parameters corresponding to the BE, width, and intensity of the quasiparticle peaks for different polarizations. The Fermi function $f(E,T)$ is evaluated for room temperature, the spectral function $A_{k\,i}(E_i,\omega_i)$ approximated by Lorentzian functions, and $B_k(E)$ assumed to be a Shirley-like background.[94] Here the subindex k denotes the $\mathbf{k}_\perp$ points. The full width at

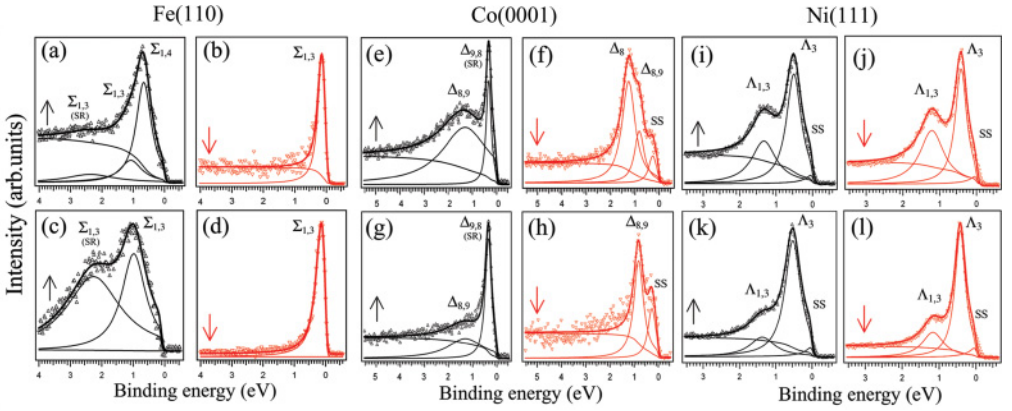

FIG. 8. (Color online) (Left panels) Fits to spin-resolved valence band spectra at $0.21\Gamma N$ ($h\nu = 35$ eV) of the Fe(110) BBZ for p polarization [(a) and (b)] and s polarization [(c) and (d)]. (Middle panels) Same for Co(0001) at $x = 0.62\ \Gamma A$ ($h\nu = 56$ eV) of the BBZ, but for p polarization [(e) and (f)] and for s polarization [(g) and (h)]. (Right panels) Same for Ni(111) at $x = 0.01\ \Gamma L$ ($h\nu = 28$ eV) of the BBZ, but for p polarization [(i) and (j)] and for s polarization [(k) and (l)]. Upward black (dark) and downward red (light) triangles and arrows for majority and minority spin spectra, respectively. Black (dark) and red (light) solid lines represent the corresponding fit results. Symmetry labels, surface resonance (SR), and surface state (SS) features are indicated.

half maximum (FWHM) of the Gaussian slit function $G(h\nu)$ corresponds to the total energy resolution ΔE_{tot} of the experiment, which is photon energy dependent.

Figure 8 shows several selected spin-dependent fits calculated for Fe, Co, and Ni spin-resolved experimental spectra and emphasizes the effect of matrix elements in each one of the experimental spin components independently. The fits obtained for p polarization are presented in the upper panel; the lower panel visualizes the corresponding fits for s-polarized light. Figures 8(a)–8(d) are devoted to Fe, Figs. 8(e)–8(h) show the Co fits, and Figs. 8(i)–8(l) represent the fits of the experimental Ni spectra, respectively. It should be mentioned that such fits are not unproblematic due to the strong energy dependence of $\text{Im}\Sigma$ which leads to the formation of asymmetric Lorentzians. Such asymmetric line shapes can be associated with the energy-dependent damping of quasiparticle excitations and, assuming that the self-energy increases quadratically with energy, with the corresponding increase of the incoherent part of the spectral function with increasing BE.

For the fitting procedure almost degenerated bands which cannot be resolved due to the experimental energy resolution are fitted with a single peak. However, by means of polarization-dependent measurements we are able to accurately obtain the linewidth of specific bands that are nearly degenerate and cannot be resolved independently under certain light polarization conditions. This point has been discussed in detail previously[40] for the case of ferromagnetic Co(0001). The method allows us to fix the width and BE positions obtained from the fits of individual bands for a given polarization to fit the shoulders of almost degenerate bands which are observed with the opposite polarization.

The linewidths which result from this analysis are presented in Fig. 9, where we have extracted the spin-dependent experimental $\text{Im}\Sigma_{\text{exp}}$ of Fe, Co, and Ni as a function of BE and compared these numbers to the theoretical ones. The results for majority [black (dark)] and minority [red (light)] spin electrons are shown in Fig. 9(a) for Fe, in Fig. 9(b) for Co, and in Fig. 9(c) for Ni, together with the corresponding LSDA + DMFT and LSDA + 3BS calculations. The error bars have been estimated from the deviation between several fitting cycles in each spectrum and a precise χ^2 minimization. The experimental data points have been corrected for nonelectronic contributions to the linewidth with the exception of impurity scattering ($\text{Im}\Sigma_{\text{imp}} = \Gamma_{\text{imp}}/2$, where $\Gamma = \text{FWHM}$) that contributes in a trivial way by a small constant and energy-independent value to the total lifetime which on the other hand can only be determined once all

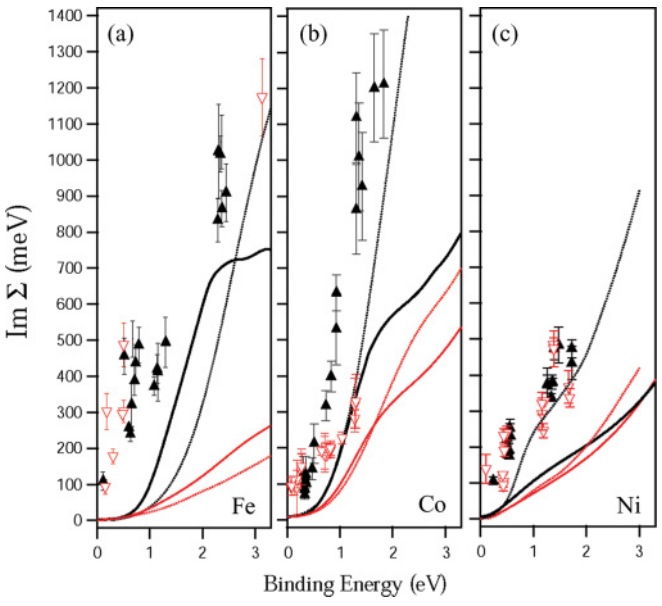

FIG. 9. (Color online) Comparison between the experimental (symbols) and theoretical (lines) imaginary parts of the self-energies of (a) Fe(110), (b) Co(0001), and (c) Ni(111) for majority [black (dark) color] and minority [red (light) color] spin electrons. The experimental data points only contain the electronic and impurity scattering contributions to the linewidth. The theoretical calculations correspond to $\text{Im}\Sigma_{\text{DMFT}}$ (thick solid lines) and to $\text{Im}\Sigma_{3BS}$ (thin dotted lines) for $U(\text{Fe}) = 1.5$ eV, $U(\text{Co}) = 2.5$ eV, and $U(\text{Ni}) = 2.8$ eV

the other contributions have been considered before. Since the broadening due to energy resolution is already included in the fitting procedure, the other experimental corrections are due to electron-phonon broadening (Γ_{e-ph}) and final-state broadening (Γ_f), where $\Gamma = 2\mathrm{Im}\Sigma$ is the scattering rate. In general, all these contributions add linearly and give a total scattering rate Γ_t such that $\Gamma_t = \Gamma_{e-e} + \Gamma_{e-ph} + \Gamma_{\mathrm{imp}} + \Gamma_f$ where Γ_{e-e} denotes the contribution to the linewidth due to electron-electron scattering.

Apparently, no quantitative agreement between the calculations and the experimental data exists but the calculations have been performed for $T = 0$ K and contain no lifetime effects due to phonon excitations. For a more realistic comparison we have to estimate the Γ_{e-ph} and Γ_f contributions to the experimental linewidths and subtract them from the total scattering rate.

A good approximation in our case could be found in the Debye model and for the high temperature limit.[95,96] Here the electron-phonon broadening depends linearly on the temperature T as $\Gamma_{e-ph} = 2Im\Sigma_{e-ph} = 2\pi\lambda k_B T$ where k_B and λ are the Boltzmann and electron-phonon coupling constants. This holds for temperatures $T \geqslant T_{\mathrm{Debye}}/3$ [T_{Debye} is 460 K (Fe), 385 K (Co), 375 K (Ni)]. From resistivity measurements[97] we derive for Fe $\lambda \approx 0.34$, for Co $\lambda \approx 0.32$, and for Ni $\lambda \approx 0.31$. This results in a $\mathrm{Im}\Sigma_{e-ph} \approx 25$ meV for Fe, Co, and Ni and indicates that the $\sim$100 meV experimental broadening observed near E_F cannot be explained by electron-phonon interaction. Furthermore, it should be pointed out that not only near E_F but also at higher BE the additional broadening observed in the experiment cannot be caused by final-state effects, since those are fully taken into account in the 1SM calculations. We have checked this point in detail by estimating the final-state broadening from the experimental data. This was done by simply unfolding the bands around the corresponding high symmetry points and by calculating the experimental electron initial and final-state group velocities assuming a free electron parabola as a final state. In a first step, the initial-state group velocities were calculated from the derivative of the $E(\mathbf{k}_\perp)$ experimental dispersions of the different majority and minority spin bands. Next, the inelastic mean free path values were taken from the semiempirical estimation given by Penn[98] and other available reference data.[99] From this estimation and due to the relatively flat dispersions of the *d* bands, we find very small ratios between the initial and final-state group velocities. These ratios result into a maximum contribution to $\mathrm{Im}\Sigma_{\mathrm{exp}}$ of $\mathrm{Im}\Sigma_f \approx$(20–30) meV due to final-state effects for all three materials. Taking into account the estimations of $\mathrm{Im}\Sigma_{e-ph}$ and $\mathrm{Im}\Sigma_f$, we come to the conclusion that the observed broadening near E_F in the experiment is due to a spin-independent impurity scattering process (i.e., $\mathrm{Im}\Sigma_{\mathrm{imp}} \sim 50$ meV in all three materials).

Figure 9 clearly demonstrates that even after we eliminate electron-phonon, final-state, and impurity scattering contributions from the experimental linewidths no quantitative agreement between the experimental and theoretical $\mathrm{Im}\Sigma$ can be obtained, but both spin channels are qualitatively reproduced by theory at least in the case of Co and Ni. We obtain to a first approximation a $\mathbf{k}$-independent $\mathrm{Im}\Sigma_{\mathrm{exp}}$ which exhibits an almost linear energy-dependent behavior. For Co the experimental data reveal the existence of a pronounced spin-dependent effect in the quasiparticle lifetimes for binding energies larger than $\sim$0.8 eV [see Fig. 9(b)], in agreement with the present calculations and previous works.[39,41]

On the other hand, in Ni [Fig. 9(c)] this effect is not present meaning that the linewidth broadening is approximately equal for both spin channels. This can be explained qualitatively by the fact that Ni has a small magnetic moment and according to this almost the same population of majority and minority spin electrons. Therefore, the possibility of creating a particle-hole pair in the minority spin channel is not much larger than for the majority spin channel. In addition, by increasing the value of U, at some point the renormalization in the minority spin channel may reach a value in which U-$J \approx U$. It is remarkable that in the case of Fe [Fig. 9(a)], $\mathrm{Im}\Sigma_{\mathrm{exp}}$ does not exhibit a spin-dependent effect, a result which is in contrast with both the 3BS and DMFT calculations. We emphasize that this may serve as an indication for an enhanced strength of spin-dependent electron correlation effects at the surface,[43] which are not considered in the present calculations. As a matter of fact we have found a strong bulk-surface coupling near E_F in the minority spin Fe states, which behave as surface resonances. For Fe majority spin states this coupling is strongly reduced giving rise to well-defined bulk structures such as the bulklike $\Sigma^{\uparrow}_{1,4}$ states we have described. Note that for Co most of the structures are well-defined bulk peaks at least within a BE range of 0.8–1.8 eV where we observe the largest spin dependence of $\mathrm{Im}\Sigma_{\mathrm{exp}}$. At binding energies below $\sim$0.4 eV, on the other hand, neither in the experiment nor in the calculations we resolve differences between the scattering rates of Co majority and minority spin electrons, in agreement with recent observations.[42] In this respect, we mention that local exchange scattering contributions[42] are qualitatively considered in our calculations via an interaction-like expansion which determines the self-energy.

Comparing Fe and Co the overall agreement between the experimental and the theoretical results is better for the latter, indicating that in the case of Co, the role of nonlocal correlations is not as important as for Fe.[31] This also holds for nonlocal spin-flip exchange scattering processes because they are not included in our calculations. These effects, on the other hand, seem to be strongly reduced inspecting Ni. To approximate the Ni bulk structures by introducing $\mathrm{Im}\Sigma_{\mathrm{exp}}$ as a k-independent function works even better than for Fe and Co. On the other hand, in Ni the difference is that surface emission is much more important and both majority and minority spin channels exhibit the largest bulk-surface coupling of the three materials. Because in Ni surface emission extends in relatively wide BE range, we expect that enhanced correlation effects at the surface of this material may introduce an extra broadening mechanism which is independent from nonlocal fluctuations. In this respect, our results are consistent with a reduction of the nonlocality of correlation effects but also with an increase of bulk-surface coupling with increasing atomic number. This fact may also serve as a test for enhanced electron correlation effects at the surface of these materials.

Finally, we would like to mention that the deviations between experimental and theoretical data of Fig. 9 seem to be equally pronounced for both spin channels but the theoretical $\mathrm{Im}\Sigma$ underestimates the experimental values in all three cases

by roughly a factor of 2. In the LSDA + DMFT calculations, this discrepancy is even more pronounced at higher binding energies. In general, $\mathrm{Im}\Sigma_{\mathrm{DMFT}}$ and $\mathrm{Im}\Sigma_{3BS}$ agree well for the same U values, on the other hand, in particular for Ni, they deviate at higher binding energies. This can be attributed to the fact that LSDA + 3BS calculations explicitly include electron-hole pair excitations, whereas our LSDA + DMFT calculations are based on a FLEX solver which includes electron-hole pair excitations in a qualitative sense only. We expect that such deviations between both methods will disappear by using a quantum Monte Carlo solver in the corresponding LSDA + DMFT and LSDA + 3BS calculations.

V. SUMMARY

We have presented a detailed comparison between spin- and angle-resolved photoemission experiments and state-of-the-art theoretical calculations of the three prototypical ferromagnetic 3*d*-tansition metals Fe, Co, and Ni. Experimentally, we have examined in detail the properties of different bulklike and surface-related spin-polarized *d* bands in these systems and carried out an experimental evaluation of the mass renormalization at high binding energies. The corresponding theoretical analysis consists of a combination of DFT-LDA and many-body techniques for the electronic structure calculations with a fully relativistic spectroscopical analysis to account for multiple-scattering, matrix-elements final-state, and surface-related effects. The agreement between experiment and theory was found to be significantly improved compared to plain LSDA-based calculations. We conclude that local many-body Coulomb interactions play an important role for a quantitative description of correlation effects in Fe, Co, and Ni but more sophisticated many-body calculations are still needed to reach better agreement with experiments. At first, the layer dependence of the self-energy has been neglected in our theoretical analysis. This may be considered in future studies via self-consistent electronic structure calculations of a semi-infinite stack of atomic layers resulting thereby in a layer-dependent self-energy. In particular one would expect, especially for Ni and Co where surface related emission counts as a substantial part of the total intensity distribution, quantitative improvements in the relative intensities due to the layer dependence of the Coulomb potential, and the self-energy. The consideration of nonlocal interactions of different strength but also the existence of nonlocal spin-flip exchange scattering processes are still needed to improve the agreement between theory and experiment, in particular concerning the linewidths and the dispersion behavior of the different electronic states. Nonlocal electron correlations are caused by long-range electron-electron interactions and have been completely neglected in our calculations. These effects result in **k**-dependent self-energies Σ_{DMFT} or Σ_{3BS} which most probably would lead to a much better agreement between theory and experiment. The fact that nonlocal correlations can have a certain influence on the intermediate energy states is closely related to previously reported results for Fe and Co.[31,40] In addition, the study of satellite structures in Fe and Co seems to be a realistic option using a nonlocal layer-dependent self-energy calculated from a self-consistent combination of cluster-DMFT with the LSDA method. Another possibility to overcome this limitation is the dual fermion approach.[100] Alternatively, it would be an important step to implement into realistic electronic structure calculations the recently proposed parameter-free extended DMFT + GW scheme,[101] in which both the on-site and off-site correlations are included. To summarize, an adequate combination of these methods should result in the near future in a even more satisfying and rather complete description of the electronic structures of Fe, Co, and Ni.

ACKNOWLEDGMENTS

This work was supported by the Deutsche Forschungsgemeinschaft (Grants No. EBE-154/18 and No. FOR1346) and the Bundesministerium für Bildung und Forschung (Grants No. 05KI0WW1/2 and No. 05KSIWMB/1).

[1] H. Wadati, T. Yoshida, and A. Fujimori, Lect. Notes Phys. **715**, 327 (2007).
[2] J. Fink, S. Borisenko, A. Kordyuk, A. Koitzsch, J. Geck, V. Zabolotnyy, M. Knupfer, B. Büchner, and H. Berger, Lect. Notes Phys.**715**, 295 (2007).
[3] A. Sekiyama, S. Imada, A. Yamasaki, and S. Suga, Lect. Notes Phys.**715**, 351 (2007).
[4] C. Herring, in *Magnetism*, Vol. VI, edited by G. T. Rado and H. Suhl (Academic Press, New York, 1966).
[5] E. W. Plummer and W. Eberhardt, Adv. Chem. Phys. **49**, 533 (1982).
[6] F. J. Himpsel, Adv. Phys. **32**, 1 (1983).
[7] R. Feder, *Polarized Electrons in Surface Physics* (World Scientific, Singapore, 1985).
[8] L. C. Davis, J. Appl. Phys. **59**, R 25 (1986).
[9] S. D. Kevan, *Angle Resolved Photoemission, Theory and Current Applications* (Amsterdam, Elsevier, 1992).
[10] M. Donath, Surf. Sci. Rep. **20**, 251 (1994).
[11] S. Hüfner, *Photoelectron Spectroscopy: Principles and Applications* (Springer, New York, 1995).
[12] O. Rader and W. Gudat, in *Numerical Data and Functional Relationships in Science and Technology*, Landolt-Börnstein, New Series, Group III Vol. 23C2, edited by A. Goldmann (Springer, Berlin, 1999).
[13] P. D. Johnson and G. Güntherodt, in *Handbook of Magnetism and Advanced Magnetic Materials*, edited by H. Krönmuller and S. Parkin (John Wiley and Sons, New York, 2007).
[14] S. Hüfner, *Very High Resolution Photoelectron Spectroscopy* (Springer, New York, 2007).
[15] V. L. Moruzzi, A. R. Williams, and J. F. Janak, *Calculated Electronic Properties of Metals* (Pergamon Press, Oxford, 1977).
[16] J. P. Perdew and Y. Wang, Phys. Rev. B **33**, 8800 (1986).
[17] A. Georges, G. Kotliar, W. Krauth, and M. J. Rozenberg, Rev. Mod. Phys. **68**, 13 (1986).

[18] M. I. Katsnelson and A. I. Lichtenstein, J. Phys.: Condens. Matter. **11**, 1037 (1999).

[19] A. I. Lichtenstein, M. I. Katsnelson, and G. Kotliar, Phys. Rev. Lett. **87**, 067205 (2001).

[20] C. Calandra and F. Manghi, Phys. Rev. B **50**, 2061 (1994).

[21] D. E. Eastman, F. J. Himpsel, and J. A. Knapp, Phys. Rev. Lett. **40**, 1514 (1978).

[22] F. J. Himpsel, J. A. Knapp, and D. E. Eastman, Phys. Rev. B **19**, 2919 (1979).

[23] W. Eberhardt and E. W. Plummer, Phys. Rev. B **21**, 3245 (1980).

[24] J. Braun, J. Minár, H. Ebert, M. I. Katsnelson, and A. I. Lichtenstein, Phys. Rev. Lett. **97**, 227601 (2006).

[25] J. Minár, H. Ebert, C. DeNadaï, N. B. Brookes, F. Venturini, G. Ghiringhelli, L. Chioncel, M. I. Katsnelson, and A. I. Lichtenstein, Phys. Rev. Lett. **95**, 166401 (2005).

[26] J. Bünemann, F. Gebhard, T. Ohm, R. Umstätter, S. Weiser, W. Weber, R. Claessen, D. Ehm, A. Harasawa, A. Kakizaki, A. Kimura, G. Nicolay, S. Shin, and V. N. Strocov, Europhys. Lett. **61**, 667 (2003).

[27] A. Santoni and F. J. Himpsel, Phys. Rev. B **43**, 1305 (1991).

[28] J. Schäfer, M. Hoinkis, E. Rotenberg, P. Blaha, and R. Claessen, Phys. Rev. B **72**, 155115 (2005).

[29] A. L. Walter, J. D. Riley, and O. Rader, New J. Phys. **12**, 013007 (2010).

[30] J. Schäfer, D. Schrupp, E. Rotenberg, K. Rossnagel, H. Koh, P. Blaha, and R. Claessen, Phys. Rev. Lett. **92**, 097205 (2004).

[31] J. Sánchez-Barriga, J. Fink, V. Boni, I. Di Marco, J. Braun, J. Minár, A. Varykhalov, O. Rader, V. Bellini, F. Manghi, H. Ebert, M. I. Katsnelson, A. I. Lichtenstein, O. Eriksson, W. Eberhardt, and H. A. Dürr, Phys. Rev. Lett. **103**, 267203 (2009).

[32] M. M. Steiner, R. C. Albers, and L. J. Sham, Phys. Rev. B **45**, 13272 (1992).

[33] F. J. Himpsel and D. E. Eastman, Phys. Rev. B **21**, 3207 (1980).

[34] D. E. Eastman, F. J. Himpsel, and J. A. Knapp, Phys. Rev. Lett. **44**, 95 (1980).

[35] J. Osterwalder, J. Elec. Spec. Rel. Phenom. **117**, 71 (2001).

[36] M. Getzlaff, J. Bansmann, J. Braun, and G. Schönhense, J. Magn. Magn. Mater. **161**, 70 (1996).

[37] C. Math, J. Braun, and M. Donath, Surf. Sci. **482**, 556 (2001).

[38] F. J. Himpsel and D. E. Eastman, Phys. Rev. B **20**, 3217 (1979).

[39] S. Monastra, F. Manghi, C. A. Rozzi, C. Arcangeli, E. Wetli, H. J. Neff, T. Greber, and J. Osterwalder, Phys. Rev. Lett. **88**, 236402 (2002).

[40] J. Sánchez-Barriga, J. Minár, J. Braun, A. Varykhalov, V. Boni, I. Di Marco, O. Rader, V. Bellini, F. Manghi, H. Ebert, M. I. Katsnelson, A. I. Lichtenstein, O. Eriksson, W. Eberhardt, H. A. Dürr, and J. Fink, Phys. Rev. B **82**, 104414 (2010).

[41] M. Mulazzi, J. Miyawaki, A. Chainani, Y. Takata, M. Taguchi, M. Oura, Y. Senba, H. Ohashi, and S. Shin, Phys. Rev. B **80**, 241106 (2009).

[42] A. Goris, K. M. Döbrich, I. Panzer, A. B. Schmidt, M. Donath, and M. Weinelt, Phys. Rev. Lett. **107**, 026601 (2011).

[43] A. Grechnev, I. Di Marco, M. I. Katsnelson, A. I. Lichtenstein, J. Wills, and O. Eriksson, Phys. Rev. B **76**, 035107 (2007).

[44] J. Bünemann, W. Weber, and F. Gebhard, Phys. Rev. B **57**, 6896 (1998).

[45] X.-Y. Deng, L. Wang, X. Dai, and Z. Fang, Phys. Rev. B **79**, 075114 (2009).

[46] G. C. Burnett, T. J. Monroe, and F. N. Dunning, Rev. Sci. Instrum. **65**, 1893 (1994).

[47] H. Fritzsche, J. Kohlhepp, and U. Gradmann, J. Magn. Magn. Mater. **148**, 154 (1995).

[48] I.-G. Baek, H. G. Lee, H.-J. Kim, and E. Vescovo, Phys. Rev. B **67**, 075401 (2003).

[49] M. Farle, A. Berghaus, Yi Li, and K. Baberschke, Phys. Rev. B **42**, 4873 (1990).

[50] A. Rampe, D. Hartmann, and G. Güntherodt, in *Spin-Orbit-Influenced Spectroscopies of Magnetic Solids*, edited by W. Beiglböck (Springer, Berlin, 1996).

[51] A. Bettac, J. Bansmann, V. Senz, and K. H. Meiwes-Broer, Surf. Sci. **454**, 936 (2000).

[52] J. B. Pendry, Surf. Sci. **57**, 679 (1976).

[53] G. Borstel, Appl. Phys. A **38**, 193 (1985).

[54] C. Caroli, D. Lederer-Rozenblatt, B. Roulet, and D. Saint-James, Phys. Rev. B **8**, 4552 (1973).

[55] J. Korringa, Physica **6/7**, 392 (1947); W. Kohn and N. Rostocker, Phys. Rev. **94**, 1111 (1954); A. R. Williams and J. van Morgan, J. Phys. C **7**, 37 (1974); R. G. Brown and M. Ciftan, Phys. Rev. B **27**, 4564 (1983); X.-G. Zhang, A. Gonis, and J. M. MacLaren, *ibid.* **40**, 3694 (1989); W. H. Butler and R. K. Nesbet, *ibid.* **42**, 1518 (1990); H. Ebert and B. L. Gyorffy, J. Phys. F **18**, 451 (1988); S. C. Lovatt, B. L. Gyorffy, and G. Y. Guo, J. Phys.: Condens. Matter **5**, 8005 (1993); R. Feder, J. Phys. C **14**, 2049 (1981).

[56] J. Braun, Rep. Prog. Phys. **59**, 1267 (1996).

[57] J. Braun, in *Band-Ferromagnetism: Ground-State and Finite-Temperature Phenomena*, edited by K. Baberschke, M. Donath, and W. Nolting (Springer, Berlin, 2001), p. 267.

[58] J. B. Pendry, *Low Energy Electron Diffraction* (Academic, London, 1974).

[59] G. Hilgers, M. Potthoff, N. Müller, U. Heinzmann, L. Haunert, J. Braun, and G. Borstel, Phys. Rev. B **52**, 14859 (1995).

[60] J. Minár, L. Chioncel, A. Perlov, H. Ebert, M. I. Katsnelson, and A. I. Lichtenstein, Phys. Rev. B **72**, 045125 (2005).

[61] G. Kotliar and D. Vollhardt, Phys. Today **57**, 53 (2004).

[62] A. K. Rajagopal and J. Callaway, Phys. Rev. B **7**, 1912 (1973).

[63] M. V. Ramana and A. K. Rajagopal, Adv. Chem. Phys. **54**, 231 (1983).

[64] P. Strange, H. Ebert, J. B. Staunton, and B. L. Györffy, J. Phys.: Condens. Matter **1**, 2959 (1989).

[65] G. Kotliar, S. Y. Savrasov, K. Haule, V. S. Oudovenko, O. Parcollet, and C. A. Marianetti, Rev. Mod. Phys. **78**, 865 (2006).

[66] K. Held, Adv. Phys. **56**, 829 (2007).

[67] L. V. Pourovskii, M. I. Katsnelson, and A. I. Lichtenstein, Phys. Rev. B **72**, 115106 (2005).

[68] M. Cococcioni and S. de Gironcoli, Phys. Rev. B **71**, 035105 (2005).

[69] S. Chadov, J. Minár, M. I. Katsnelson, H. Ebert, D. Ködderitzsch, and A. I. Lichtenstein, Europhys. Lett. **82**, 37001 (2008).

[70] V. I. Anisimov and O. Gunnarsson, Phys. Rev. B **43**, 7570 (1991).

[71] A. Hofmann, X. Y. Cui, J. Schäfer, S. Meyer, P. Höpfner, C. Blumenstein, M. Paul, L. Patthey, E. Rotenberg, J. Bünemann, F. Gebhard, T. Ohm, W. Weber, and R. Claessen, Phys. Rev. Lett. **102**, 187204 (2009).

[72] J. Hermanson, Solid State Commun. **22**, 9 (1977).

[73] R. L. Benbow, Phys. Rev. B **22**, 3775 (1980).

[74]T. Okuda, J. Lobo-Checa, W. Auwärter, M. Morscher, M. Hoesch, V. N. Petrov, M. Hengsberger, A. Tamai, A. Dolocan, C. Cirelli, M. Corso, M. Muntwiler, M. Klöckner, M. Roos, J. Osterwalder, and T. Greber, Phys. Rev. B **80**, 180404(R) (2009).
[75]F. Reinert, G. Nicolay, S. Schmidt, D. Ehm, and S. Hüfner, Phys. Rev. B **63**, 115415 (2001).
[76]F. Aryasetiawan, M. Imada, A. Georges, G. Kotliar, S. Biermann, and A. I. Lichtenstein, Phys. Rev. B **70**, 195104 (2004).
[77]S. Hüfner, Phys. Lett. A **51**, 299 (1975).
[78]C. Guillot, Y. Ballu, J. Paigné, J. Lecante, K. P. Jain, P. Thiry, R. Pinchaux, Y. Pétroff, and L. M. Falicov, Phys. Rev. Lett. **39**, 1632 (1977).
[79]R. Clauberg, W. Gudat, W. Radlik, and W. Braun, Phys. Rev. B **31**, 1754 (1985).
[80]A. Kakizaki, K. Ono, K. Tanaka, K. Shimada, and T. Sendohda, Phys. Rev. B **55**, 6678 (1997).
[81]K. N. Altmann, D. Y. Petrovykh, G. J. Mankey, N. Shannon, N. Gilman, M. Hochstrasser, R. F. Willis, and F. J. Himpsel, Phys. Rev. B **61**, 15661 (2000).
[82]J. Osterwalder, J. Elec. Spec. Rel. Phenom. **117–118**, 71 (2001).
[83]N. Kamakura, Y. Takata, T. Tokushima, Y. Harada, A. Chainani, K. Kobayashi, and S. Shin, Phys. Rev. B **74**, 045127 (2006).
[84]O. Karis, S. Svensson, J. Rusz, P. M. Oppeneer, M. Gorgoi, F. Schäfers, W. Braun, W. Eberhardt, and M. Mårtensson, Phys. Rev. B **78**, 233105 (2008).
[85]A. Liebsch, Phys. Rev. Lett. **43**, 1431 (1979).
[86]A. Liebsch, Phys. Rev. B **23**, 5203 (1981).
[87]O. Miura and T. Fujiwara, Phys. Rev. B **77**, 195124 (2008).
[88]C. S. Wand and J. Callaway, Phys. Rev. B **15**, 298 (1977).
[89]J. Kanski, P. O. Nilsson, and C. G. Larsson, Solid State Commun. **35**, 397 (1980).
[90]Y. Sakisaka, T. Komeda, M. Onchi, H. Kato, S. Masuda, and K. Yagi, Phys. Rev. B **36**, 6383 (1987).
[91]T. Kinoshita, T. Ikoma, A. Kakizaki, T. Ishii, J. Fujii, H. Fukutani, K. Shimada, A. Fujimori, T. Okane, and S. Sato, Phys. Rev. B **47**, 6787 (1993).
[92]N. Nakajima, S. Hatta, J. Odagiri, H. Kato, and Y. Sakisaka, Phys. Rev. B **70**, 233103 (2004).
[93]D. Benea, J. Minár, L. Chioncel, S. Mankovsky, and H. Ebert, Phys. Rev. B **85**, 085109 (2012).
[94]D. A. Shirley, Phys. Rev. B **5**, 4709 (1972).
[95]N. W. Ashcroft and N. D. Mermin, *Solid State Physics* (Saunders College, Philadelphia, 1976).
[96]A. V. Fedorov, T. Valla, F. Liu, P. D. Johnson, M. Weinert, and P. B. Allen, Phys. Rev. B **65**, 212409 (2002).
[97]P. B. Allen, Phys. Rev. B **36**, 2920 (1987).
[98]D. R. Penn, Phys. Rev. B **35**, 482 (1987).
[99]W. S. M. Werner, K. Glantschnig, and C. Ambrosch-Draxl, J. Phys. Chem. Ref. Data **38**, 1013 (2009).
[100]A. N. Rubtsov, M. I. Katsnelson and A. I. Lichtenstein, Phys. Rev. B **77**, 033101 (2008).
[101]S. Biermann, F. Aryasetiawan, and A. Georges, Phys. Rev. Lett. **90**, 086402 (2003).